Short-term displacement of Planktothrix rubescens (cyanobacteria) in a pre-alpine lake observed using an autonomous sampling platform

Garneau, Marie-Ève ; Posch, Thomas ; Hitz, Gregory ; Pomerleau, François ; Pradalier, Cédric ; Siegwart, Roland ; Pernthaler, Jakob

Abstract: Short-term changes in temporal and spatial distributions of the toxic cyanobacterium Planktothrix rubescens in Lake Zurich were investigated using high-resolution data sets acquired with an autonomous surface vessel (ASV). Data profiles were recorded with a multi-parameter probe while the ASV navigated along 1.5 km toward a waypoint located on the other side of the lake by using a global positioning system. We deployed the ASV seven times on five consecutive days during the stratification period (July 2011) to generate cross-sectional views of temperature, light, oxygen, and phycoerythrin and chlorophyll fluorescence from surface to 18 m. The data were also used to compute daily photosynthetic rates. Data showed a daily reshaping of the P. rubescens distribution in the metalimnion on both horizontal and vertical axes, from patches to a shore-to-shore spreading. A thermocline depression observed after 16 h of sustained winds forced the accumulation of P. rubescens on the downwind shore. The compression of the metalimnion and its downward shift by 6 m within 24 h suggested the modulation of a longitudinal seiche following the wind event. This passive transport of the metalimnetic P. rubescens population resulted in a 90% light reduction, and a decrease of the averaged daily photosynthetic rate from +21 mmol O2 m−2 d−1 to −10 mmol O2 m−2 d−1. Negative photosynthetic rates were computed on 2 d out of 5 d, meaning that the transport of P. rubescens by seiches significantly affected the balance between oxygen production and utilization in Lake Zurich, especially because it is the dominant primary producer.

DOI: https://doi.org/10.4319/lo.2013.58.5.1892

Limnol. Oceanogr., 58(5), 2013, 1892–1906

doi:10.4319/lo.2013.58.5.1892

Short-term displacement of *Planktothrix rubescens* (cyanobacteria) in a pre-alpine lake observed using an autonomous sampling platform

Marie-Ève Garneau,[1,*] Thomas Posch,[1] Gregory Hitz,[2] François Pomerleau,[2] Cédric Pradalier,[2] Roland Siegwart,[2] and Jakob Pernthaler [1]

[1] Limnological Station Kilchberg, Institute of Plant Biology, University of Zurich, Zurich, Switzerland
[2] Autonomous Systems Lab, Swiss Federal Institute of Technology (ETH) Zurich, Zurich, Switzerland

Abstract

Short-term changes in temporal and spatial distributions of the toxic cyanobacterium *Planktothrix rubescens* in Lake Zurich were investigated using high-resolution data sets acquired with an autonomous surface vessel (ASV). Data profiles were recorded with a multi-parameter probe while the ASV navigated along 1.5 km toward a waypoint located on the other side of the lake by using a global positioning system. We deployed the ASV seven times on five consecutive days during the stratification period (July 2011) to generate cross-sectional views of temperature, light, oxygen, and phycoerythrin and chlorophyll fluorescence from surface to 18 m. The data were also used to compute daily photosynthetic rates. Data showed a daily reshaping of the *P. rubescens* distribution in the metalimnion on both horizontal and vertical axes, from patches to a shore-to-shore spreading. A thermocline depression observed after 16 h of sustained winds forced the accumulation of *P. rubescens* on the downwind shore. The compression of the metalimnion and its downward shift by 6 m within 24 h suggested the modulation of a longitudinal seiche following the wind event. This passive transport of the metalimnetic *P. rubescens* population resulted in a 90% light reduction, and a decrease of the averaged daily photosynthetic rate from +21 mmol O_2 m^{-2} d^{-1} to −10 mmol O_2 m^{-2} d^{-1}. Negative photosynthetic rates were computed on 2 d out of 5 d, meaning that the transport of *P. rubescens* by seiches significantly affected the balance between oxygen production and utilization in Lake Zurich, especially because it is the dominant primary producer.

In the pre-alpine Lake Zurich, Switzerland, the species *Planktothrix rubescens* dominates the biomass of primary producers (Micheletti et al. 1998; Bossard et al. 2001). The ecological success of *P. rubescens* lies in its adaptation to the seasonal stratification that takes place in the clear mesotrophic waters of Lake Zurich (Walsby and Schanz 2002). Not only does *P. rubescens* thrive in the metalimnion during late summer and early autumn, but the cyanobacterium also outcompetes other phytoplankton species under the low-irradiance conditions that prevail in that layer by maximizing the absorption of green light with phycoerythrin pigments (Davis and Walsby 2002; Oberhaus et al. 2007). *P. rubescens* can also regulate its buoyancy with gas vesicles to maintain and adjust its vertical position according to the irradiance, preferably at depths above its photosynthetic compensation point where it has the biggest competitive advantage (Walsby et al. 2001). The prevalence of *P. rubescens* in Lake Zurich, a drinking water reservoir for 1.5 million people, is a serious issue because it produces cyclic hepatotoxins called microcystins, including the very acute form [D-Asp^3,(*E*)-Dhb^7]microcystin-RR (Blom et al. 2001). Microcystins represent major threats to domestic animals as well as considerable hazards for human health through water consumption and bathing (Codd et al. 2005). Even though programs for water quality restoration by nutrient control have been undertaken since the 1950s in Lake Zurich (Bossard et al. 2001), *P. rubescens* populations have shown no reduction, but rather an increase during the past decades (Posch et al. 2012).

The spatial distribution of cyanobacteria varies vertically as well as horizontally in shallow (Moreno-Ostos et al. 2009; Pobel et al. 2011) and in deep lakes (Cuypers et al. 2010; Salcher et al. 2011). In the epilimnion, spatial variations may occur on short time scales (i.e., from hours to days) because most of these changes arise from meteorological conditions. For example, during quiet days of minimal mixis, cyanobacteria can form surface scums (Huisman and Hulot 2005), and whenever winds generate surface currents, these scums may accumulate locally (Pobel et al. 2011). In the metalimnion, physical changes may also arise from weather-forced events, such as when steady winds blow over a stratified lake and pile up surface waters at the lee end shore (Boegman 2009). This water buildup pushes down the thermocline on the leeward shore and creates a compensatory upward movement of the isotherms at the windward shore (Horn et al. 1986). Once winds stop, the thermal layers of the lake slide over each other to redistribute a new equilibrium generating an oscillation, called an internal seiche, which produces vertical movements of water at depth, but produces very little motion at the surface (Boegman 2009). These short-term, wind-induced events generate vertical displacements of metalimnetic populations of cyanobacteria, causing episodic changes in the irradiance that reaches the cells, which in turn modify photosynthetic rates with cascading effects on the ecosystem of small and large lakes (Cuypers et al. 2010; Pannard et al. 2011).

Short-term variations in the vertical distribution of *P. rubescens* due to displacement by seiches have been scarcely

* Corresponding author: me.garneau@gmail.com

Fig. 1. The autonomous sampling vessel, which is a catamaran 2.5 m long and 1.8 m wide called *Lizhbeth,* during a sampling mission on Lake Zurich. The winch system is used to lower a light sensor and a multi-parameter probe, which is inserted in the plane-shaped fiberglass casing. The casing has elongated perforations to allow the water to reach the sensors. The front tip of the casing is a 4.2 kg steel weight.

documented (Thomas and Märki 1949; Thomas 1950; Cuypers et al. 2010; Carraro et al. 2012), and there is no information on the variations in light conditions that are experienced by *P. rubescens* in situ. Comprehensive calculations indicated that vertical shifts significantly affect the net photosynthetic production balance because this metalimnetic population is located close to its photosynthetic compensation point (Walsby et al. 2001). Nonetheless, the ecological effects of such punctual events are poorly described because the rapid and occasional nature of their advent hinders their documentation using traditional sampling methodologies. More studies demonstrate the effectiveness of high-frequency data sampling by fixed fluorometer probes to monitor harmful cyanobacterial blooms (Leboulanger et al. 2002; Brient et al. 2008; McQuaid et al. 2011) but broader spatial information is still limited (Porter et al. 2009).

A promising avenue to address harmful cyanobacteria ecology from both a spatial and a temporal angle is the application of autonomous mobile robots which, when equipped with multiple sensors, can accurately and rapidly measure limnological parameters at biologically relevant spatiotemporal scales. The field of autonomous mobile robotics has gained more interest in autonomous surface vessels (ASV), and an increasing number of platforms are designed for lake-ecosystem studies (Caron et al. 2008; Dunbabin et al. 2009; Ferri et al. 2011). So far, none of these mobile deployments have specifically aimed for the monitoring of harmful cyanobacteria. Our newly designed ASV provides a sampling method for high temporal and spatial resolutions, both horizontally and vertically, and is thereby applicable to the variability of lake hydrology and of microbiological processes. The vessel holds a custom-designed winch employed to lower a commercial multi-parameter probe (Fig. 1). It can be rapidly deployed in Lake Zurich, thereby allowing for the monitoring of short-term variations in *P. rubescens* distribution.

Our objective was to document the role of episodic lake-water movements on the light-based positioning of *P. rubescens* in the water column and the consequences for its growth. We hypothesized that physical processes substantially affect the net photosynthetic rate of the *P. rubescens* population. We deployed our ASV to measure the underwater irradiance and to locate depths where *P. rubescens* stratified, and we then compared the measured values with the theoretical depth where the daily insolation would support its neutral buoyancy.

Methods

Study site and sample collection—Lake Zurich (Fig. 2) is a large and deep mesotrophic lake ($\sim$ 10–20 μg L^{-1} total phosphorus) located at 406 m above sea level on the Swiss Plateau, at the northern edge of the Alps (Bossard et al. 2001). The lake has a surface area of 68 km^2, a maximal depth of 136 m (Bossard et al. 2001), and 30 km long thalweg path (i.e., the deepest continuous line in the lake channel; Horn et al. 1986). The lake basin is mainly exposed to northeasterly and southwesterly winds, which are stormy in winter and spring (MeteoSwiss; http://www.meteoswiss.admin.ch/files/kd/normwerte/norm8110/windrosen/fr/SMA.pdf). Summer and autumn are comparatively calm, but various local winds circulate from the surrounding hills toward the lake at night, and from the lake back to the hills during daytime (Hantke et al. 1979). Summertime is also characterized by short episodes of strong west winds and thunderstorms that usually occur in the late afternoon (Hantke et al. 1979). The wind stress at the surface of the lake is non-uniform and quite variable because of changes in the orientation in the thalweg direction and the surrounding topography, resulting in several longitudinal internal seiche modes in Lake Zurich (Horn et al. 1986).

Meteorological parameters were obtained from the website of the Zurich Water Police (Zurich Wasserschutzpolizei, http://www.tecson-data.ch/zurich/seepozh/mythenquai.html). Continuous records of global solar irradiance (Kipp and Zonen CM3 pyranometer in W m^{-2}), wind speed (m s^{-1}), and wind direction ($^\circ$) were measured at 10 min intervals from 10 July, which is the day prior sampling, to 17 July. The weather station is located at 4.1 km north of the sampling transect (Fig. 2) and meteorological data are presented in Fig. 3.

Robotic approaches and water sampling—The ASV collected vertical data profiles using a YSI-6600 multi-parameter probe (YSI Incorporated) equipped with an array of sensors while it navigated autonomously along a linear path following pre-defined global positioning system (GPS) waypoints. The precise GPS-based navigation ensured that the positions of the measurements are reproducible from one sampling run to the other, which permitted data comparisons between all runs. The conception and manufacturing of the platform, the software design as well as the robotic aspects are fully described in Hitz et al. (2012). The navigation speed for sampling was set for maximal data coverage of the studied area while

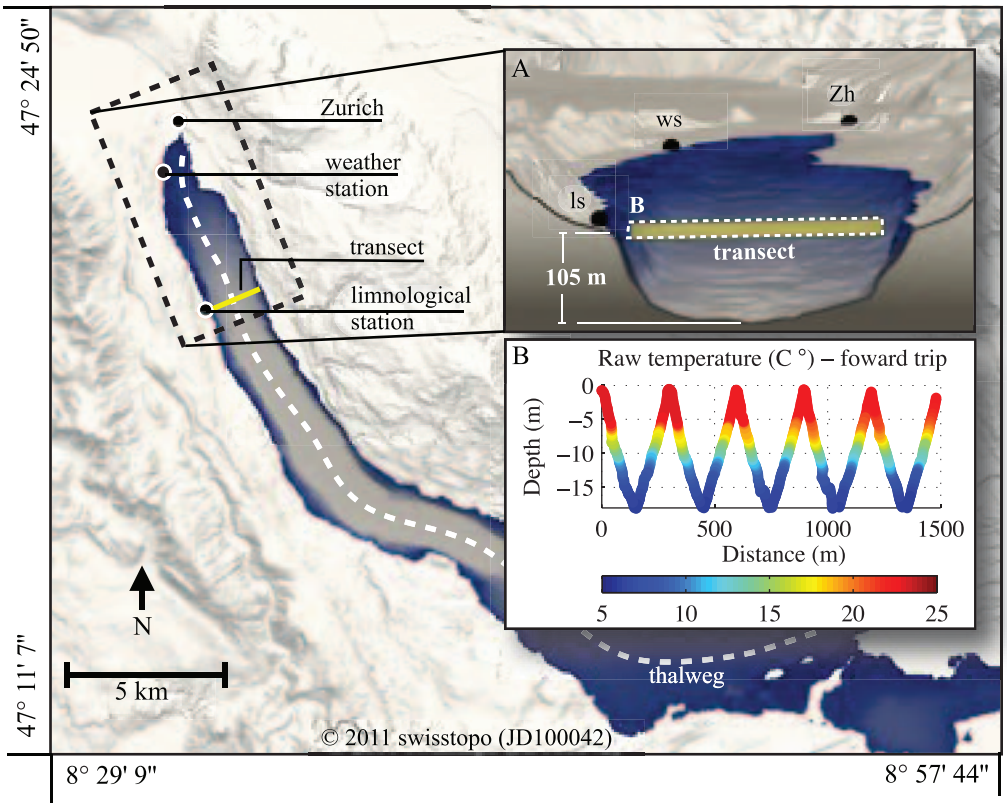

Fig. 2. Map of Lake Zurich, Switzerland, and its surrounding topography (Source: *Bundesamt für Landestopografie swisstopo* [Art. 30 GeoIV]: 5704 000 000). Also shown are the location of the sampling transect, the weather station, and the thalweg path. (A) Schematic illustration of the 1.5 km transect in Lake Zurich, where the probe is lowered and raised between 2 and 18 m. Zh stands for Zurich, ws for weather station, and ls for limnological station. (B) Plot of the raw data recorded by the temperature sensor during the forward trip toward the east shore that illustrates the zigzag path of the probe.

considering hardware-related constraints, such as the sensor measurement frequencies and the capacity of the two batteries. A sailing speed of 0.7 m s^{-1} and a vertical deployment speed of 0.1 m s^{-1} for the probe, which measures at a rate of 0.5 Hz, was the most advantageous trade-off for a round-trip sampling from east to west along the 1.5 km transect (Fig. 2A). The ASV sailed the transect in 40 min while alternately lowering and raising the probe, from the surface layer down to the upper part of the hypolimnion (2–18 m), to capture the entire metalimnion layer where *P. rubescens* accumulates during summer and autumn. The combination of the horizontal and vertical motions of the probe results in a zigzag sampling path (Fig. 2B). For a given sampling run, the raw measurements of the two inverse zigzag paths of the probe (i.e., one on the forward trip and another on the return trip) were combined to enhance the spatial coverage and to increase the accuracy of the interpolation method (details below). A complete field survey took 80 min, which is $< 10\%$ of the shortest seiche period (17 h) in Lake Zurich (Horn et al. 1986).

The sampling campaign took place from 12 to 16 July 2011 along a straight-line transect starting on the west shore (47.320119°N, 8.554894°E), and ending on the east shore (47.326092°N, 8.572475°E; Fig. 2). The ASV was deployed daily, and two times on 12 and 14 July to evaluate the variations that may occur within a day. Sampling took place ~ 2 h before and after noon, which was when the sun was at its zenith and when the irradiance was maximal. The bell-shaped curves of irradiance indicated that the light at 10:00 h and 15:00 h was usually similar (Fig. 3B). Environmental data were collected every 2 s using sensors for depth (m), temperature (°C), dissolved oxygen concentration (mg L^{-1}) and saturation level (%), chlorophyll fluorescence (relative fluorescence unit, RFU), which is a proxy for the total phytoplankton biomass, and finally for phycoerythrin fluorescence (also in RFU), which is a proxy for *P. rubescens* biomass. Additionally, a spherical quantum sensor (LI-COR) was installed on the probe to measure the in situ photosynthetically active radiation (PAR; μmol m^{-2} s^{-1}). A second sensor placed on the boat measured the PAR above the surface for reference. All sensors were calibrated according to the manufacturer's guidelines. Delays in the response of the sensors on the multi-parameter probe were detected because we were deploying them at a faster speed than recommended by YSI Incorporated. The time delay for a measurement was 15 s with the sensor for dissolved oxygen, 14 s for the phycoerythrin sensor, and 2 s for the temperature sensor. The delays in the sensor responses were easily adjusted back to the correct position of the reading, but it was not possible for the dissolved oxygen 6562 Rapid Pulse™

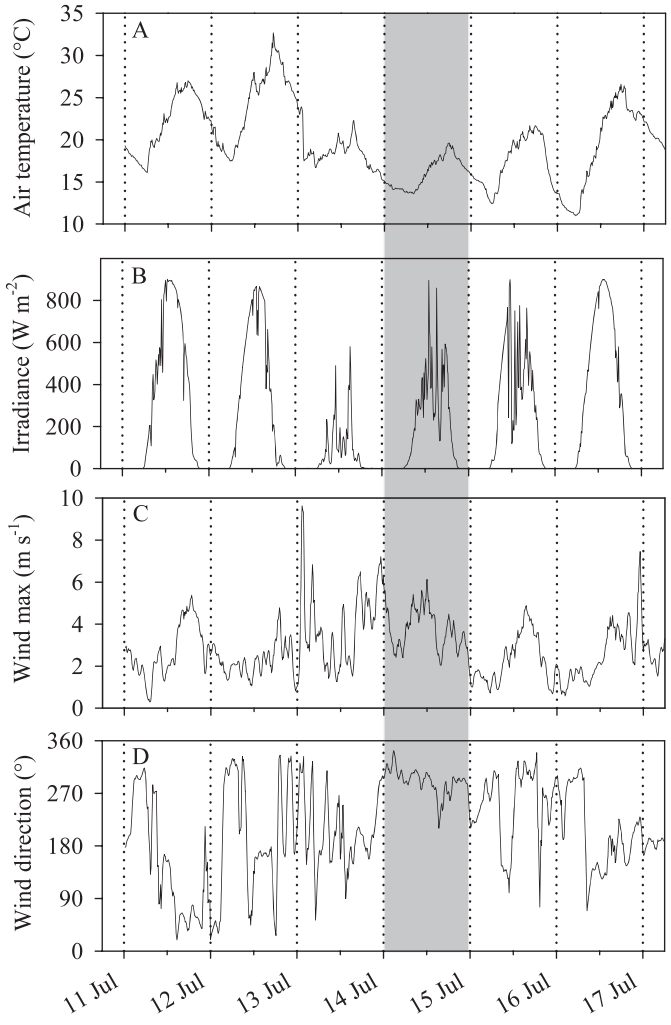

Fig. 3. Meteorological data measured from July 11, 00:00 h to July 17, 23:50 h. Presented are running means of the data recorded every 10 min for (A) air temperature, (B) solar irradiance, (C) wind speed maxima, and (D) wind direction (0° = 360° = north, 90° = east, 180° = south, 270° = west). The grey-shaded area represents the period when sustained winds blew from the northwest for 16 h.

Sensor (an electrochemical sensor) when the probe was moving upward. As a result, the values were inaccurate, and this half of the data set was excluded. A likely explanation for inaccurate oxygen values is that the sensor may respond poorly when passing from a lower oxygen zone to higher oxygen zone. Electrochemical oxygen sensors are influenced by oxygen concentration, as well as changes in temperature, salinity, pressure, and stirring (Tengberg et al. 2003). Thus, the number of data collected (n) from 2 m to 18 m with each sensor amounted to 13,904 (or $>$ 1900 for each sampling run); whereas, the data collected with the dissolved oxygen sensor (n_{DO}) was 6851.

On the first day of the sampling campaign and 1 week after, on 19 July, vertical algal pigment profiles were recorded using a TS-16-12 fluoroprobe (bbe Moldaenke GmbH) that was deployed from a small craft above the deepest point of the lake (47.307011°N, 8.577167°E). The fluoroprobe was calibrated to differentiate between green algae, diatoms, cryptophytes, and *P. rubescens*.

Quantification of Planktothrix *by quantitative PCR for sensor calibration*—The RFU values given by the phycoerythrin fluorescence sensor were considered good estimators of *P. rubescens* biovolume because its phycoerythrin content was shown to be relatively constant throughout seasons (Ernst et al. 2009) and under various light conditions (Skulberg and Skulberg 1985). The sensor was thus calibrated by associating the RFU reading at a given depth to the actual *P. rubescens* abundance, which was determined by quantitative PCR (qPCR) analysis on water samples taken at that same depth. We collected 47 samples at various depths from 0 m to 20 m from 24 March to 03 November 2011. For each depth, two 400 mL volumes were filtered through glass fiber filter membranes. The filters were processed as crude lysates, as in Garneau et al. (2011), and filtered through a 0.22 μm, low-binding cellulose acetate syringe-tip filters to efficiently remove cellular debris and filter remnants. The *P. rubescens* filaments were quantified following the qPCR TaqMan assay on the 16S ribosomal deoxyribonucleic acid (rDNA) gene developed by Ostermaier and Kurmayer (2009). The qPCR approach was calibrated using a four-point 1 : 10 serial dilutions of DNA extracts of a *P. rubescens* culture (strain A7 isolated from Lake Zurich by A. E. Walsby), for which the initial biovolume was 375 mm^3 L^{-1} ($\pm$ 126 mm^3 L^{-1}, n = 7). This concentration was determined by microscopic examination of formaldehyde-fixed filaments collected onto black polycarbonate filters (0.22 μm pore size). The autofluorescent filaments under green light were quantified by automated image analysis (Zeder et al. 2010). Counts were translated into biovolumes (Van den Wyngaert et al. 2011).

Calibration curves were loaded for each qPCR run of unknown samples to directly translate threshold cycle (C_t) values into biovolumes. The calibration curve spanned over concentrations from 3.75×10^0 mm^3 L^{-1} to 3.75×10^{-3} mm^3 L^{-1}, which corresponded to 2.34×10^{-5} mm^3 to 2.34×10^{-8} mm^3 of filaments per qPCR reaction. Six calibration curves were run and combined to give a master calibration curve described as $y = -3.24x + 9.36$, $r^2 = 0.96$. The qPCR efficiency (E) was calculated as $E = 100 \times 10^{(-1/m)} - 1$ (where m is the slope of the master calibration curve) and equaled 103%, which is within the acceptable range of 90–110% for assay validation (Invitrogen 2008). The qPCR method accuracy was confirmed by comparing qPCR results with microscopic slides counted in triplicate for 11 lake samples. The standard deviation on biovolumes determined by microscopy was, on average, 30%. For a given sample, the standard deviation on the triplicate qPCR runs was, on average, 16%, and was never above 30%. Correlation analysis showed that the two quantification methods gave very similar abundance values (m = 0.82, r^2 = 0.93). The linear regression used to convert RFU values into qPCR-based biovolume (BioV in mm^3 L^{-1}) was BioV = 0.806 [RFU] $-$ 0.899 (r^2 = 0.90, n = 47, $p \leq 0.05$).

Data interpolation—Sensor data were post-processed using a two-dimensional interpolation method to create a

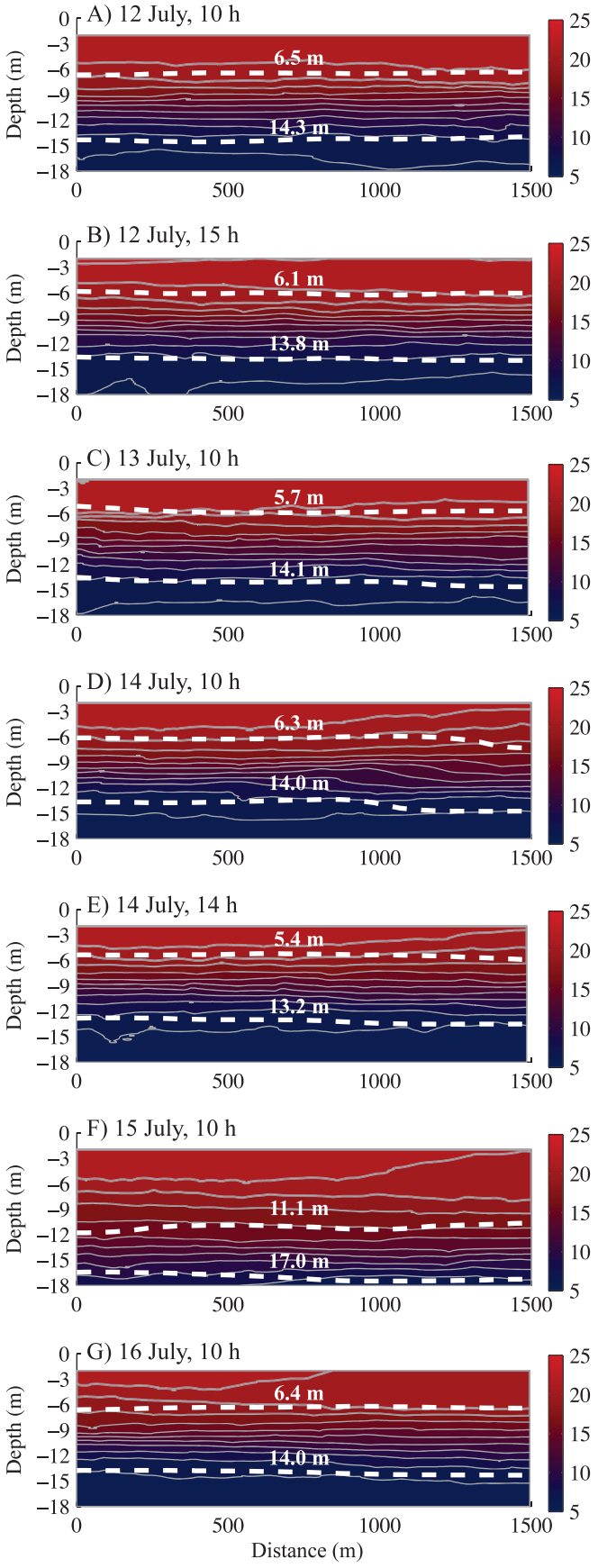

cross-sectional representation. These cross sections were shaped using an anisotropic distance kernel because there was a large difference between the scale of the horizontal axis (1.5 km) and the vertical axis (18 m). Interpolations were calculated over a depth range of 2–18 m using MATLAB. This interpolation procedure was evaluated, and results indicated that the error of the interpolation is contained within the temporal variability observed in the field (Hitz et al. 2012). For a given environmental parameter, each interpolated value is considered representative of a volume that has a length of 30 m, a width of 30 m, and a height of 0.6 m. Using the interpolated temperature profiles, the thermocline stratification index (TSI in °C m^{-1}) was computed as follows:

$$TSI = \Delta T / \Delta h \quad (1)$$

where ΔT is the difference in water temperature and Δh is the depth interval (Yu et al. 2010). The stratification increases with TSI values. The metalimnion boundaries displayed on Figs. 4 and 5 were determined using a gradient value of > 1°C m^{-1}.

Calculations of daily insolation, neutral buoyancy depth, and photosynthetic compensation point—Two different irradiance sensors were used in this study: (1) a quantum LI-COR sensor, which measured the in situ PAR (or visible range, 400–700 nm) in μmol m^{-2} s^{-1}; and (2) a radiometric Kipp and Zonen CM3 pyranometer, which measured the global solar spectrum (305–2800 nm) in W m^{-2} at the surface of the lake. The conversion of these radiometric units into photon units was estimated by the LI-COR manufacturer to be roughly 4.6 μmol m^{-2} s^{-1} $\approx$ 1 W m^{-2}, which is equivalent to 1 J m^{-2} s^{-1} (Biggs 2000). Because about 46% of the total solar energy is emitted in the visible range (Walsby 2001; Blumthaler 2012), a value of 1 J m^{-2} s^{-1} on the CM3 pyranometer should be equivalent to 2.116 μmol m^{-2} s^{-1} on the LI-COR sensor (i.e., 4.6 μmol m^{-2} s^{-1} $\times$ 0.46). Thus, we used the theoretical ratio LI-COR : CM3 of 2.116 μmol J^{-1} (i.e., 2.116 μmol m^{-2} s^{-1} : 1 J m^{-2} s^{-1}) to convert the pyranometer values into PAR equivalent values.

Each 10 min record of the global solar irradiance was first multiplied by 600 s (i.e., 10 min = 10 $\times$ 60 s) to transform values in J m^{-2}. The resulting values were afterward multiplied by 2.116 μmol J^{-1}. The daily irradiance at the water surface Q_0 (in mol m^{-2}) was then calculated from the sum of the 10 min records over a period of 24 h. The daily insolation Q_z at depth z was calculated as follows:

←

Fig. 4. Cross-sectional views of temperature (in °C) along the transects across Lake Zurich between 12 and 16 July 2011, indicated by letters A to G. The dashed white lines indicate the upper and lower boundaries of the metalimnion, and depths indicated on each line are mean values computed over the full transect. The thin grey lines are the temperature isolines.

$$Q_z = Q_0 \frac{I_z}{I_0} \quad (2)$$

where I_z is the irradiance at depth z and I_0 is the irradiance measured just below the water surface, both in μmol m^{-2} s^{-1}.

The neutral buoyancy depth z_N is defined as the depth where 50% of the *P. rubescens* filaments naturally float, which corresponds to the depth where the daily photon insolation Q_N is equal to 0.28 mol m^{-2} (Walsby et al. 2004), and is calculated as follows:

$$z = z_I + \Delta z \frac{\ln\left(\frac{Q_I}{q}\right) - \ln\left(\frac{Q}{q}\right)}{\ln\left(\frac{Q_I}{q}\right) - \ln\left(\frac{Q_{I+1}}{q}\right)} \quad (3)$$

where $z = z_N$ and $Q = Q_N$; Δz is the sampling depth interval; q is a constant equal to 1 mol m^{-2}; z_I and z_{I+1} are, respectively, sampling depths immediately above and below the depth where the insolation equals Q_N; and Q_I and Q_{I+1} are the daily insolation at these depths.

The growth compensation point E_g was defined as the irradiance in the light phase that supports no growth over a cycle of 12 h of light and 12 h of darkness (Davis and Walsby 2002). A E_g value of 0.8245 μmol m^{-2} s^{-1} was determined for a *P. rubescens* culture growing at 15°C during 12 h of light (Davis and Walsby 2002). To obtain the daily photon insolation Q_C that corresponds to the compensation point for *P. rubescens* growth, the E_g value was multiplied by 43,200 s (equivalent to 12 h), which gives a resulting Q_C value of 0.0356 mol m^{-2}. The compensation depth z_C is calculated using Eq. 3 where $z = z_C$ and $Q = Q_C$. Interpolated data were used to calculate z_N and z_C for each sampling run. The resulting data were depicted in Fig. 5.

Calculation of the daily integrals of photosynthesis—Daily integrals of photosynthesis were computed using our vertical profile measurements of *P. rubescens* biovolumes, temperature, and irradiance in Lake Zurich, and following the calculation procedures of Walsby (1997, 2001). The relationship between photosynthesis P and irradiance I is described as follows:

$$P = P_m \left[1 - \exp\left(\frac{-\alpha I}{P_m}\right)\right] + R + \beta I \quad (4)$$

where P is the photosynthetic rate, P_m is the maximum photosynthetic rate, and R is the rate at zero irradiance (all in μmol cm^{-3} h^{-1}); α is the initial slope of the P/I curve at low irradiance and β is the P/I curve slope at high irradiance (both in μmol cm^{-3} h^{-1}[μmol m^{-2} s^{-1}]$^{-1}$); and I is the photon irradiance in μmol m^{-2} s^{-1}.

The photosynthetic coefficients α, β, P_m, and R were determined experimentally by Walsby et al. (2001), where R was the standardized respiration R_s calculated as $-0.11 \times P_m$ (set 1 in Table 1). Among the photosynthetic coefficients available in the literature, the coefficients from Walsby et al. (2001) were the most relevant to our data set for three reasons: (1) the coefficients were measured for a natural population of *P. rubescens* in Lake Zurich; (2) the samples were incubated at 11 m in Lake Zurich, which reflects the in situ light and temperature T' of 15.5°C; and (3) values are means of four P/I curves measured at different time points to account for daily variations in the coefficients. The daily photosynthetic rates computed with the parameter set 1 were considered default values. They were compared to rates computed using two other sets of parameters, also determined for *P. rubescens* from Lake Zurich (Table 1). The coefficient set 2 was calculated from cultures growing at 20°C under controlled light conditions (Walsby 2001); whereas, the set 3 was calculated from resuspended filaments collected in the lake and incubated at 12°C (Micheletti et al. 1998).

The photosynthetic rates P_{zt} (in μmol m^{-3} h^{-1}) for a given depth z at a given time t were computed from the potential rate of photosynthesis that is predicted by the photosynthetic coefficients and the in situ irradiance measurements. Irradiance I_{tz} at a given depth z and time t is given as follows:

$$I_{tz} = I_{0t}\left[\frac{I_z}{I_0}\right] \quad (5)$$

where I_{0t} is the irradiance below the surface at time t. The parameter I_{tz} replaced I in Eq. 4, which is re-arranged as follows:

$$P_{zt} = B_z \left[P_m\left(1 - \exp\left(\frac{-\alpha I_{tz}}{P_m}\right)\right) + R + (\beta I_{tz})\right] T_{10}^{\left(\frac{(T_z - T')}{10}\right)} \quad (6)$$

where B_z is *P. rubescens* biovolume at depth z (in cm^3 m^{-3}). Equation 6 also incorporates a correction term for temperature, where $T_{10} = 2$ and is the relative increase in P over 10°C; T' is the incubation temperature for the P/I curves (given in Table 1), and T_z is the temperature measured at depth z.

We used the interpolated data to compute P_{zt}. The interpolation gave a value for a volume that has a length of 30 m, a width of 30 m, and a height of 0.6 m. In other words, the 1.5 km (or 1500 m) transect is composed of 50 interpolated volumes on the horizontal axis (distance) and 27 interpolated volumes on the vertical axis (depths from 2 m to 18 m). This sequence of interpolated areas can be seen as a series of consecutive columns aligned from the west shore to the east shore of the lake, over a distance range of 0 m to 1500 m. Thus, for a given column, we calculated a P_{zt} value for each depth z at each time point t. Then, double integrals $\sum\sum(P)$ over a day (24 h) and throughout depths (from 2 m to 18 m) were calculated with the trapezoidal rule. Daily integral photosynthetic rates are expressed in mmol O_2 m^{-2} d^{-1} and are estimators of the photosynthesis by *P. rubescens* during a day in a given surface area of Lake Zurich, from the surface down to the upper part of the hypolimnion. The transects also have a horizontal dimension (i.e., the distance); therefore, a mean value was calculated for each transect.

Statistical analysis—Statistical analyses on sensor data were performed using MATLAB. The data were not following a normal distribution; therefore, we used non-parametric tests. Medians and interquartile ranges ($Q1$ and

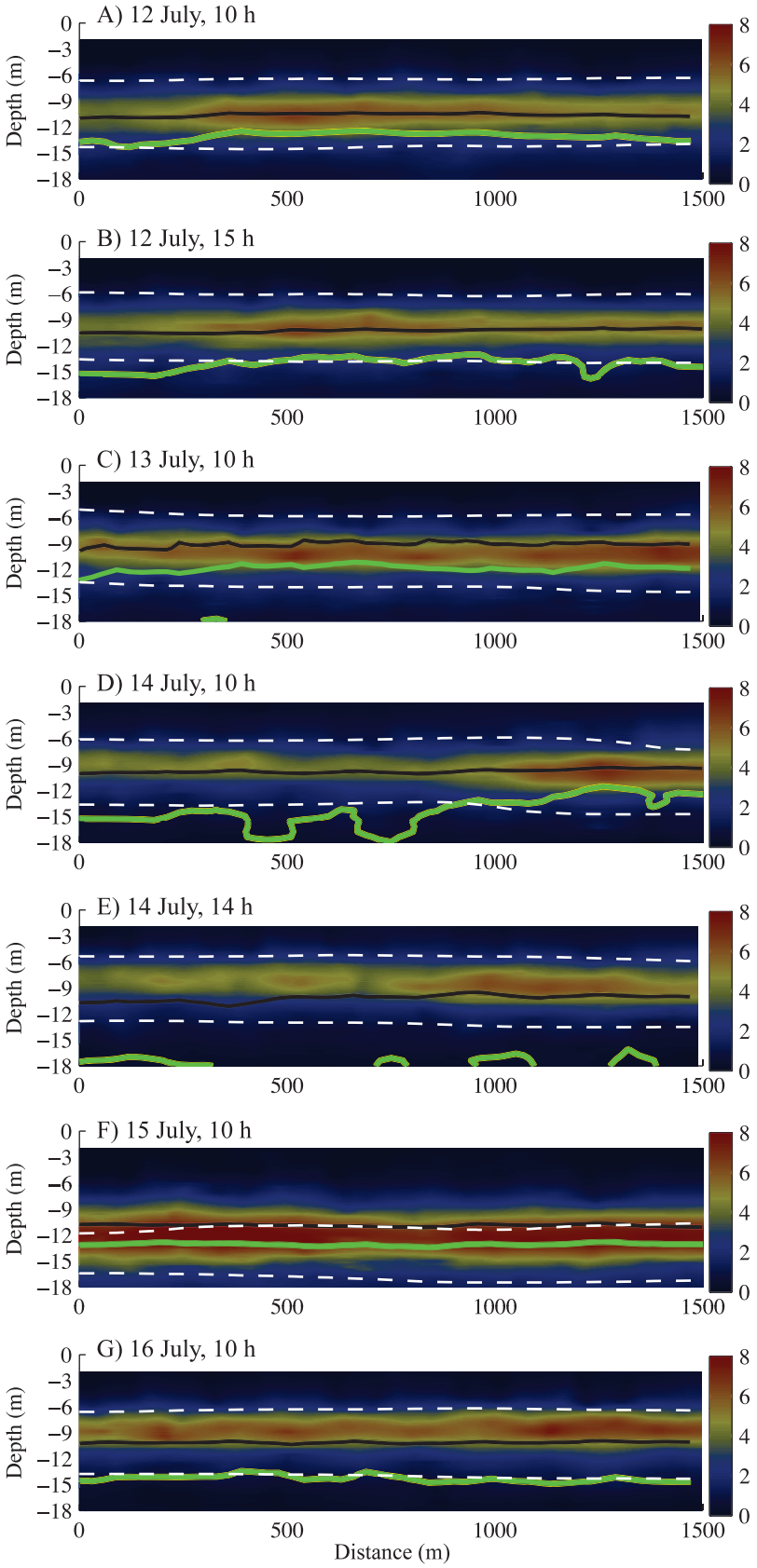

	West shore	Center	East shore
Prub	3.2	**3.9****	3.2
Temp	12.8	13.1	12.7
I	**7.1***	**4.9***	6.4
DO%	102	108	105
n (n_{DO})	328 (199)	403 (213)	322 (111)
Prub	3.3	**3.7****	3.1
Temp	11.8	12.7	13.3
I	**6.9***	6.5	**6.4***
DO%	99	103	105
n (n_{DO})	379 (214)	377 (198)	318 (109)
Prub	**3.3***	3.6	**3.8***
Temp	13.7	**13.2***	**13.6***
I	2.4	**1.9***	**3.4***
DO%	104	105	107
n (n_{DO})	381 (209)	378 (197)	326 (121)
Prub	2.6	2.9	**3.9****
Temp	12.7	12.0	13.7
I	2.9	2.8	**2.2****
DO%	**90***	100	**105***
n (n_{DO})	304 (185)	367 (196)	296 (107)
Prub	**2.8****	3.1	3.4
Temp	12.2	**11.6***	**13.0***
I	**6.3***	**3.4***	5.0
DO%	89	95	**100****
n (n_{DO})	305 (185)	375 (192)	312 (116)
Prub	**5.4***	**4.7***	5.4
Temp	12.6	12.4	12.9
I	0.5	**0.5***	**0.5***
DO%	100	95	95
n (n_{DO})	275 (161)	312 (155)	264 (107)
Prub	**2.9****	**3.3****	**3.8****
Temp	**10.6***	12.6	**13.3***
I	4.8	6.5	7.0
DO%	**81****	93	98
n (n_{DO})	340 (213)	367 (201)	298 (98)

Table 1. Photosynthetic coefficient sets for *Planktothrix rubescens* of Lake Zurich. Set 1 was used to compute the default value of daily integral photosynthetic rates; the two other sets are for comparison. Coefficients were measured from experimental determination of *P/I* curves (i.e., the relationship between photosynthesis *P* and irradiance *I*) of *P. rubescens* that was incubated in situ (set 1) or in controlled conditions using cultures (set 2) or resuspended filaments in lake water (set 3). *See* Methods section for details on each photosynthetic coefficient.

Coefficient and unit	Set 1*	Set 2†	Set 3‡
α (μmol cm^{-3} h^{-1} (μmol m^{-2} s^{-1}) $^{-1}$)	26.7	14.9	88.2
β (μmol cm^{-3} h^{-1} (μmol m^{-2} s^{-1}) $^{-1}$)	0.522	−0.0797	−0.269
P_m (μmol cm^{-3} h^{-1})	676	486	1472.4
R (μmol cm^{-3} h^{-1})	−74	−47.3	−100.3
T' (°C)	15.5	20.0	12.9
T_{10}	2	2	2

* Walsby et al. 2001.
† Walsby 2001.
‡ Micheletti et al. 1998.

*Q*3) were used to summarize each sampling run as well as each lake layer. The relationship between two variables was evaluated based on Spearman's rank correlation coefficient (r_S) at the level of significance $p < 0.05$. Kruskal–Wallis analyses on rank-ordered data (KW) were used to compare data between different groups. The null hypothesis that mean ranks of samples were the same for all the groups was rejected when $p < 0.05$. First, the three layers of the lake were compared: (1) epilimnion, (2) metalimnion, and (3) hypolimnion. Data were grouped by layer according to the metalimnion depths determined using Eq. 1. Values from 2 m to the upper edge of the metalimnion were allocated to the epilimnion; whereas, values from the lower edge of the metalimnion down to 18 m were assigned to the hypolimnion. Analyses were performed for each sampling run separately and for all the data together. Second, KW tests were also performed for each sampling run to determine whether the data recorded in the metalimnion in three different areas of the lake come from the same population. The three areas were (1) west shore or windward shore (0–500 m), (2) central lake area (500–1000 m), and (3) east shore or leeward shore (1000–1500 m). Finally, KW tests were used to examine temporal variations by comparing the seven sampling runs (Figs. 4A–G, 5A–G). Dunn's post-hoc tests were used to determine which layers, areas, or runs differed from each other. It is worth noting that unlike the one-way analysis of variance, the KW analysis does not test the null hypothesis that the populations have equal means or medians. This implies that two groups having identical medians or means could be significantly different if their mean ranks are different (McDonald 2009).

Results

Meteorological and physico-chemical parameters—The weather during the week of sampling was fluctuating, and when clouds appeared on 13 July, the air temperature and the irradiance decreased accordingly (Fig. 3A,B). On 14 July, steady winds of moderate intensity accompanied by gusts of up to 7 m s^{-1} blew from the northwest for more than 16 continuous hours (Fig. 3C,D). On 15 July, the winds subsided, the temperature gradually rose, and the next day was sunny (Fig. 3). Temperature profiles showed that Lake Zurich was thermally stratified throughout the sampling campaign (Fig. 4). Statistical analysis confirmed that the epi-, meta-, and hypolimnion layers were significantly different in terms of temperature, dissolved oxygen saturation level, and in situ irradiance, whether considering all the data or each sampling run separately (KW $p < 0.05$; Table 2). All data taken together indicated that between 12 and 16 July, the median temperature in the metalimnion was 12.8°C and the median oxygen concentration was 11.4 mg L^{-1}, equivalent to a median of 99% of saturation. The light intensity in the metalimnion amounted to 3.5 μmol m^{-2} s^{-1} (Table 2). Comparatively, the median light intensity was much higher (median 207 μmol m^{-2} s^{-1}) in the epilimnion, and much lower (median 0.60 μmol m^{-2} s^{-1}) in the upper part of the hypolimnion (Table 2).

Biovolumes of P. rubescens—Vertical profiles of pigments recorded with the fluoroprobe indicated that *P. rubescens* was the dominant primary producer in Lake Zurich during the sampling period (Fig. 6). *P. rubescens*

←

Fig. 5. Cross-sectional views of *P. rubescens* biovolume (in cm^3 m^{-3}) in Lake Zurich between 12 and 16 July 2011. The dashed white lines indicate the upper and lower boundaries of the metalimnion. The black line indicates the depth of the neutral buoyancy (z_N), while the green line indicates the depth of the compensation point for growth (z_C). The right panel presents corresponding median values in the metalimnion for *Planktothrix* biovolumes (Prub), temperature (Temp), underwater irradiance (*I*), and dissolved oxygen saturation (DO%) calculated from the sensor data in each of the three transect areas for a given sampling run. The areas of the metalimnion that were significantly different (Kruskal–Wallis analysis [KW], $p < 0.05$) for a given variable are in bold. A double asterisk indicates an area that differs from all other areas; whereas, a single asterisk indicates two areas that are significantly different (KW $p < 0.05$). *n* indicates the size of the data sets for Temp, *I,* and Prub, and n_{DO} is the size of the DO data set.

Table 2. Median values and interquartile ranges ($Q1$ and $Q3$, in italics) for temperature (Temp), underwater irradiance (I), *Planktothrix rubescens* biovolumes (Prub), and dissolved oxygen (DO) in the epilimnion, the metalimnion, and the upper hypolimnion from 12 to 16 July 2011. Values were calculated from sensor data that were recorded over the entire lake transect. All the layers were significantly different (Kruskal–Wallis analysis, $p < 0.05$) than the other layers for all variables, except for two variables. n indicates the size of the data sets for Temp, I, and Prub; and n_{DO} indicates the size of the DO data set.

Layer	n	Temp (°C)	I (μmol m^{-2} s^{-1})	Prub (cm^3 m^{-3})	n_{DO}	DO (mg L^{-1})	DO (%)
Epilimnion	3230	*20.7*–21.5–*21.9*	*90*–207–*410*	*0.23*–0.63–*1.4**	1530	*10.8*–11.2–*11.5**	*118*–121–*125*
Metalimnion	7018	*9.55*–12.8–*16.5*	*1.2*–3.5–*18*	*2.2*–3.4–*4.9*	3487	*10.1*–11.4–*11.9**	*81*–99–*112*
Upper hypolimnion	3656	*6.11*–6.40–*6.84*	*0.30*–0.60–*0.80*	*0.55*–0.79–*1.1**	1834	*7.6*–7.9–*8.3*	*61*–63–*66*

* Indicates the two layers that *are not* significantly different from each other ($p > 0.05$) for Prub and for DO.

accounted on average for 57% of the total chlorophyll *a* concentration, whereas the second most abundant group, the diatoms, accounted for 38%. No cryptophytes, which also contain phycoerythrin pigments, were detected (Fig. 6). *P. rubescens* filaments were well-stratified in the metalimnion, where highest biovolumes were found (Table 2). The median biovolumes in the epi- and hypolimnion were similarly low, and were significantly different from the biovolumes of the metalimnion (KW $p < 0.05$; Table 2). When considering the *P. rubescens* biovolume data of all runs and all layers together, the only strong correlation (i.e., $r_S > 0.60$) found was with chlorophyll fluorescence ($r_S = 0.75$, $p < 0.05$), concordant with the observation that this organism was the dominant autotroph in the lake at the time of sampling. There was also an association between oxygen concentration and *P. rubescens* ($r_S = 0.48$, $p < 0.05$), showing the importance of *P. rubescens* as primary producer. This is in keeping with the recent work of Salcher et al. (2011), who demonstrated that *P. rubescens* was the dominant primary producer at the scale of the lake. The association with oxygen increased when considering the total chlorophyll fluorescence (i.e., all the primary producers in the top 18 m [$r_S = 0.84$, $p < 0.05$]).

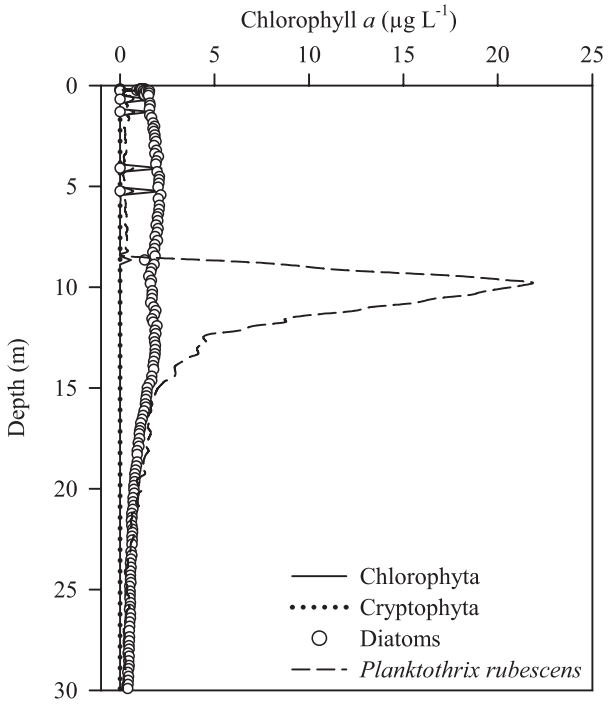

Fig. 6. Depth profiles of four phytoplankton groups in the upper water column of Lake Zurich on 19 July 2011. The concentration of each algal group is expressed in μg chlorophyll *a* L^{-1}. No cryptophytes were detected.

When the three layers were analyzed separately, more correlations were found. The epilimnion data subset indicated that *P. rubescens* was more abundant as we go deeper in the epilimnion (*P. rubescens* vs. depth, $r_S = 0.76$) where underwater irradiance (I), temperature (temp), and dissolved oxygen saturation level (DOsat) were lower (*P. rubescens* vs. I, $r_S = -0.64$; vs. temp, $r_S = -0.77$; vs. DOsat, $r_S = -0.59$; $p < 0.05$). The metalimnion subset showed a stronger association between *P. rubescens* and the dissolved oxygen concentration ($r_S = 0.53$, $p < 0.05$) than when all data were considered.

Spatial and temporal variations in the metalimnion—Most filaments were confined into a distinctive *Planktothrix* layer (Fig. 5) that moved according to the oscillations of the metalimnion (Fig. 4). The metalimnion width and location changed within a day but, on average, the upper boundary was located at 6.8 ± 2.0 m while the lower boundary was at 14.4 ± 1.2 m. Cross-sectional views also revealed horizontal heterogeneity in isotherm depths, metalimnion widths (Fig. 4), and *P. rubescens* biovolumes (Fig. 5). The metalimnion tended to be slightly larger on the east shore than on the west shore, and this was particularly apparent on 15 July (Fig. 4F). Two transversal views from the first sampling day depicted a particularly dense patch of *P. rubescens* in the central portion of the lake (Fig. 5A,B). Biovolumes and underwater irradiance in the metalimnion were significantly different there than on both shores (KW $p < 0.05$; Fig. 5A,B). On the next day, 13 July, *P. rubescens* was more abundant on the east than on the west shore, as suggested by KW test showing a significant ($p < 0.05$) difference between these two areas; whereas underwater light and temperature in the central part were different from the west shore (KW $p > 0.05$; Fig. 5C).

The windy conditions that lasted 16 h during the night of 13 to 14 July (Fig. 3D) seemed to have induced the thermocline depression that was visible on the morning of 14 July (Fig. 5D). The core of the *P. rubescens* population was then located on the shore opposite to the prevailing winds (i.e., the east shore) where metalimnetic biovolumes were significantly different compared with elsewhere in the lake (KW $p < 0.05$; Fig. 5D). The over-saturating oxygen concentrations and the low underwater irradiance in the metalimnion also showed differences between the three

Table 3. Daily irradiance (Q_0), irradiance measured just below the water surface (I_0), and range of underwater irradiance (I_{meta}) in the metalimnion (median, $Q1$ and $Q3$ [in italics]). Double integrals of daily photosynthesis were computed using the parameter set 1 (DP-1), set 2 (DP-2), and set 3 (DP-3) and averaged over the transect. Also presented are the medians of sensor data measured from 2 m to 18 m for *Planktothrix* biovolumes (Prub) and dissolved oxygen saturation level (DO). Letters A to G refer to the seven sampling runs, as used in Figs. 4 and 5. Sampling runs that were significantly different (Kruskal–Wallis, $p < 0.05$) from all other sampling runs for a given variable are in bold and indicated by an asterisk (*).

Date, time	Q_0 (mol m^{-2})	I_0 (μmol m^{-2} s^{-1})	I_{meta} (μmol m^{-2} s^{-1})	Prub (cm^3 m^{-3})	DO (%)	DP-1 (mmol O_2 m^{-2} d^{-1})	DP-2 (mmol O_2 m^{-2} d^{-1})	DP-3 (mmol O_2 m^{-2} d^{-1})
A) 12 Jul, 10 h	50.0	490	*1.3*–5.9–*37*	1.8	99	23.2	8.38	141
B) 12 Jul, 15 h	50.0	440	*2.4*–6.6–*34*	1.8	95	34.0	13.1	170
C) 13 Jul, 10 h	11.5	180	*0.70*–2.4–*12*	1.6	**96***	−20.8	−11.6	39.5
D) 14 Jul, 10 h	32.2	240	*1.0*–2.6–*13*	1.4	90	12.2	3.56	105
E) 14 Jul, 14 h	32.2	340	*1.8*–4.7–*23*	1.3	**78***	29.9	11.5	156
F) 15 Jul, 10 h	41.6	490	***0.30*–0.50–*1.8****	**2.8***	**112***	−10.3	−8.29	119
G) 16 Jul, 10 h	58.1	490	*2.3*–5.8–*37*	1.3	81	76.2	32.0	284

areas of the lake (KW $p < 0.05$; Fig. 5D). In the afternoon, the biovolume on the west shore was significantly different compared with the two other areas, and temperature was higher on the east than in the center (KW $p < 0.05$; Fig. 5E). Also observed in that afternoon was the shallowest depth of the metalimnion layer (Fig. 4E). The concentrations of *P. rubescens* in the metalimnion on 14 July were slightly lower (Fig. 5D,E) when compared with all sampling runs (Table 3).

A striking change was observed on 15 July, when the metalimnion was at its deepest location (Fig. 4F) and was thinnest (average of 5.9 m). It harbored a dense and elongated *Planktothrix* layer aligned on the 12 m depth isoline that was significantly different in the central area than on the west shore (KW $p < 0.05$), but not different from the east shore (Fig. 5F). The quartiles for *P. rubescens* biomass were as follows: west shore $Q1 = 3.4$, $Q3 = 7.5$; center $Q1 = 2.6$, $Q3 = 7.2$; and east shore $Q1 = 3.1$, $Q3 = 7.5$. Similarly, even though the medians for irradiance were equal, the center differed from the east shore (KW $p < 0.05$; Fig. 5F). Quartiles were as follows: west shore $Q1 = 0.30$, $Q3 = 1.5$; center $Q1 = 0.30$, $Q3 = 2.5$; east shore $Q1 = 0.20$, $Q3 = 1.4$. *P. rubescens* concentrations were maximal on 15 July; whereas, underwater light was the lowest, and accordingly, both parameters significantly differed from all other sampling runs (KW $p < 0.05$; Table 3). On 16 July, the core of the *Planktothrix* layer was shifted 3 m upward (Fig. 5G) and its biovolume was reduced when compared with the previous day (Table 3). Temperature, dissolved oxygen saturation level, and *P. rubescens* biovolume were low and all different on the west shore (KW $p < 0.05$; Fig. 5G).

Neutral buoyancy and compensation depths, and daily photosynthesis—During the sampling period, the shallowest mean depth for neutral buoyancy was 9.0 m on 13 July, and the deepest was 10.9 m on 15 July (Fig. 5). The bulk of *P. rubescens* biomass was found aligned with the neutral buoyancy depth on three occasions: twice on the sunny, warm, and calm day of 12 July, and once more on the relatively windy and cloudy morning of 14 July (Fig. 5A,B,D). On two instances, most of *P. rubescens* filaments were located above the neutral buoyancy depth (Fig. 5E,G). The compensation point was usually positioned close to the lower border of the metalimnion. Its mean value fluctuated between 12.2 m and below 18.0 m (Fig. 5). Most of the *P. rubescens* biomass was found above the compensation depth, except on 15 July, where that point was located at a mean depth of 13.1 m (Fig. 5F). The deepest compensation depth (> 18 m) was found on 14 July in the afternoon (Fig. 5E).

The daily irradiance Q_0 varied significantly during the sampling period, with values oscillating between 11.5 mol m^{-2} on 13 July to a maximum of 58.1 mol m^{-2} on the 16 July (Table 3). Daily photosynthesis (DP) calculated for each sampling run indicated that the amount of oxygen produced by *P. rubescens* varied from 12.2 mmol O_2 m^{-2} d^{-1} to 76.2 mmol O_2 m^{-2} d^{-1} (DP-1 in Table 3). Negative daily photosynthesis rates of −20.8 mmol O_2 m^{-2} d^{-1} and −10.3 mmol O_2 m^{-2} d^{-1} were computed on 13 and 15 July, respectively, indicating net oxygen consumption by *P. rubescens*. On both days, most of the *P. rubescens* biomass was located below the neutral buoyancy depth (Fig. 5C,F), even though these 2 d were different in terms of light field in the metalimnion. Solar radiation and underwater irradiance were minimal on 13 July; whereas, these values were among the highest on 15 July (Fig. 3B; Table 3), but a large portion of the biomass was located much deeper (Fig. 5F). On 15 July, the percentages of oxygen saturation and the biovolumes of *P. rubescens* were also significantly different from all the other days (KW $p < 0.05$; Table 3), and a notable proportion of *P. rubescens* biomass was found below the compensation depth (Fig. 5F). Interestingly, on 14 and 16 July, two dates after which a negative photosynthesis value was obtained, we observed oxygen saturation percentages that were lower than 100% or, in other words, a relative oxygen deficit (Table 3). The deficit in dissolved oxygen on 14 July in the afternoon (median 78%) was significantly different from all other sampling runs (KW $p < 0.05$; Table 3).

Two daily photosynthesis values were calculated for 12 and 14 July. For both days, the values calculated using the afternoon data set were 1.5–2.5 times higher than when calculated using the morning data set (Table 3). The rates seemed to follow the available light in the metalimnion,

rather than the light below the water surface at the time of the sampling (Table 3). Nonetheless, the two daily photosynthetic rates computed for a given day were of the same order of magnitude and showed the same trend for a net production. The parameter set used to compute the daily photosynthetic rates had a large influence on the resulting values (Table 3). The parameters determined on a culture grown at 20°C (set 2) yielded rates that were 30–80% lower than when using parameters determined in situ at 15°C (set 1; Table 3). Nonetheless, both parameter sets gave similar trends in the computed photosynthesis (e.g., negative rates were computed for the same days). This was not the case when using the parameter set 3, which gave much larger estimations and no negative values (Table 3).

Discussion

High-resolution depiction of P. rubescens *distribution*—The sampling at high temporal resolution highlights the rapid remodeling of the *Planktothrix* distribution under wind-forcing, on both horizontal and vertical axes. The *Planktothrix* layer was moved downward along with the oscillating metalimnion by about 6 m in < 24 h, which is much larger than the mean filament sinking velocity of 0.4–0.52 m d^{-1} (Walsby et al. 2001; Walsby and Holland 2006). The seiche-induced vertical displacement reduced the light quantity in the metalimnion by $\sim 90\%$ with effects on daily photosynthesis calculations that returned negative values, denoting oxygen consumption by *P. rubescens*. These results showed that seiche movements can sometimes move a metalimnetic population close to, or even below, its compensation depth and, thus, have consequences on the balance between oxygen production and utilization. This is especially significant in an ecosystem such as Lake Zurich, where the phytoplankton biomass is dominated by the metalimnetic cyanobacteria *P. rubescens.*

The brief but intensive sampling campaign carried out in Lake Zurich gave fine temporal observations of the *Planktothrix* layer movements from a cross-section perspective. The existence of seiche movements was inferred from the isotherm displacements at our fixed transect location, but our sampling was not designed to show the complexity of physical processes at the basin scale. Such detailed work would have required time-series data from current meters and thermistor chains fixed on several moorings (Horn et al. 1986). Our study rather intended to illustrate the effects of known physical phenomena on the ecology of *P. rubescens* in Lake Zurich. The results are among the first to depict a short-term (3 d) displacement of the *Planktothrix* layer caused by a storm event.

Robotics combined with sensing technologies had made possible the observation of seiche motions by the acquisition of high-resolution data in both space and time. These new and promising approaches for collecting continuous measurements will surely contribute to our understanding of ecosystems by generating large amounts of data at relevant but yet unexplored scales. The organization, integration, and analysis of such huge data sets are challenging, and thus new software tools intelligible to ecologists need to be developed for a better management and visualization of these high-frequency data. Technological shortcomings may also arise with the response time of the sensors when profiling at fast speed, which were particularly critical with the dissolved oxygen sensor. Oxygen optodes may be an interesting solution because they are highly precise and accurate optical sensors, and are more stable than electrochemical sensors (Tengberg et al. 2003), but so far, the response time is still too slow for fast profiling speeds. The development of better, faster sensors is necessary for rapid profiling applications, especially because a greater utilization of sensor technologies for field biology studies is foreseen (Porter et al. 2009).

Patchiness in P. rubescens *spatial distribution*—The transverse sections of Lake Zurich confirmed that *P. rubescens* stretches from the western to the eastern side of the basin, displaying a patchy pattern similar to the one observed on a longitudinal north–south transect (Salcher et al. 2011). Our results are in line with other observations of the patchiness in *P. rubescens* horizontal distribution in pre- and alpine lakes (Cuypers et al. 2010; Sotton et al. 2011). Large patches (~ 500 m long) of dense *Planktothrix* biomass recurrently formed in the metalimnion during our sampling, with apparent effects on the local physico-chemistry. In most areas where thick aggregations were present, less light was measured, dissolved oxygen was found in over saturating concentrations, and higher temperatures were recorded (Fig. 5). Local increases in dissolved oxygen are probably driven by high photosynthetic rates of an abundant cyanobacterial biomass. Compact buildup of cyanobacterial cells may also have contributed to slightly warm the area due to the light absorption by their photosynthetic pigments (Agustí and Philips 1992). In the same vein, the accumulation of *Planktothrix* filaments over a growth season was recognized as the major modulator of light attenuation in Lake Zurich (Walsby et al. 2001). Our results showed that this could also be applied to shorter time scales, because condensed biomass induced a localized steepening of the light gradient leading to self-shading. Self-shading may have an effect on toxin synthesis (Kardinaal et al. 2007). Results of the latter authors' competition experiments with *Microcystis* cultures indicated that non-microcystin-producing strains compete better for light than microcystin-producing ones. Similarly, dense, shaded patches of biomass may favor non-microcystin-producing *P. rubescens* filaments, which, even though they are more vulnerable to grazers (Kurmayer and Jüttner 1999), can hide from grazers in the toxic accretion.

At a larger scale, underwater light, and thus photosynthetic production, can be modified by cloud cover, which has an effect on the buoyancy response of the *Planktothrix* filaments. Theoretically, the neutral buoyancy depth is located where the light averaged over a day can support the photosynthetic production of dense components (i.e., carbohydrates) in moderate amounts that would still permit 50% of filaments to naturally float (Walsby et al. 2004). Fluctuations in cloud cover were shown to affect the neutral buoyancy depth on a daily basis (Walsby et al. 2004), and we also observed this within a single day. When

the sun was visible in the afternoon of 14 July, more light was measured in the water column than in the morning (Table 3), and thus the depth of z_N was pushed downward by $\sim$ 1 m on the west shore (Fig. 5D,E). Interestingly, the z_N depth stayed roughly at the same place on the east shore because of light attenuation by the denser *Planktothrix* patch. The median depth of this *Planktothrix* patch had slightly moved upward by $\sim$ 1 m during that 4 h interval. This motion indicated a relative increase of gas vesicle volume compared with the amount of photosynthesized carbohydrates, which consumption can be inferred by a concomitant decrease in oxygen saturation percentages. Still, this displacement was greater than the estimated average speed of *Planktothrix* filaments ($\sim$ 0.5 m d^{-1}), meaning that they were entrained upward along with the metalimnion. Filaments can only maintain their depth if the water column is completely stable, and their buoyancy response is delayed relative to changes in irradiance (Walsby and Schanz 2002). Hence, the *Planktothrix* layer was aligned on the theoretical neutral buoyancy depth only on some occasions of calm weather. This limitation in buoyancy capacities was already described for motile phytoplankton species living in the epilimnion, such as the harmful dinoflagellate *Ceratium*. *Ceratium* cells cannot migrate to optimal light conditions during windy days, but can form a distinct layer during calm periods, even if they last only a couple of hours (Alexander and Imberger 2009). As with *P. rubescens,* the *Ceratium* population is located at a depth of favored light conditions only for a short time each day. Whether *P. rubescens* formed a dense layer that stretched from one shore to the other or rather was localized in a patch, the filaments were moved daily below or above the calculated neutral buoyancy depth during our sampling campaign, presumably by the action of seiches.

Vertical displacements of P. rubescens *and effects on daily photosynthesis*—The vertical heterogeneity in the *Planktothrix* distribution provided further evidences for the up-and-down movements generated by wind-induced seiches. This phenomenon was recently documented for Lake du Bourget, a large and deep alpine lake, where the depth of the *Planktothrix* maximum was displaced by up to 10 m at a given sampling location within a day (Cuypers et al. 2010). In Lake Zurich, seiche motions were reported to move the thermocline and the *Planktothrix* layer by up to 2 m over 36 h (Walsby et al. 2001). We noted larger vertical movements than in this previous study, but the 6 m downward shift of the metalimnion in < 24 h is similar to observations in Lake du Bourget.

The thermocline depression and biomass accumulation observed on the east shore of Lake Zurich on 14 July were likely caused by sustained winds that blew from the northwest for 16 consecutive hours the night before. These winds could also have contributed to a modulation of the dominant longitudinal seiche in the lake, which has a period of 44 h (Horn et al. 1986), to form a seiche with two vertical motions and one horizontal motion (V2H1 seiche). Just after wind relaxation, seiches usually display one vertical and one horizontal motion; whereas, V2H1 seiches are generated as the oscillation progresses in the lake (Boegman 2009). The second vertical mode of a V2H1 seiche creates oscillations in the epilimnion and the hypolimnion that are in opposite modes, which produce alternating movements of compression and stretching of the metalimnion (Münnich et al. 1992). On two occasions, our results depicted patches in the middle of the lake that had stretched into a large band that spread shore to shore within a day. No such remodeling of the *Planktothrix* layer was previously documented in Lake Zurich, even if seiche motions were detected (Walsby et al. 2001). In a small and elongated Swiss alpine lake (5 km long and 1 km wide), a V2H1 seiche was reported to provoke a simultaneous maximal thickness of the metalimnion at one end of the lake and minimal thickness at the other end (Münnich et al. 1992). Our transversal illustrations may be snapshots of the compression and extension of the metalimnion by a V2H1 seiche that travels longitudinally, entraining *P. rubescens* filaments from north to south in the lake basin. This may explain the sudden increase in biovolume noted on 15 July (Fig. 5F). Large changes in *P. rubescens* biovolumes along the north–south longitudinal axis of Lake du Bourget were also very likely generated by two-vertical-mode seiches (Cuypers et al. 2010). Furthermore, the prevailing longitudinal mode of 44 h ($\sim$ 1.8 d) in Lake Zurich fits with our time-series of isotherms depicted in Fig. 4, showing the metalimnion at nearly the same place on the mornings of 12, 14, and 16 July. The cross-sections of *P. rubescens* biomass are two-dimensional, and thus cannot reflect the variations across the entire lake basin. Even though our data set is limited to a fixed transversal line, the sampling scheme allowed for the observation of the temporal variations in *P. rubescens* distribution that were likely occurring at the scale of the lake basin.

Vertical movements due to seiches drastically affect the depth of the metalimnion and, thus, the irradiance that can reach the *Planktothrix* layer. As pointed out previously (Walsby 2001), little alterations in the layer depth lead to substantial changes in daily photosynthesis because the *Planktothrix* population was often located at its compensation depth during our sampling. Consequently, the balance between net positive and negative daily photosynthesis had fluctuated from one day to the other. The largest variation to occur between two consecutive days was an eight-fold increase in daily photosynthetic rates from -10 mmol O_2 m^{-2} d^{-1} to 76 mmol O_2 m^{-2} d^{-1}. Seiche displacement of the *Planktothrix* layer was previously shown to induce a two-fold change in light regime, which had contributed to increase the daily photosynthesis from 9 mmol O_2 m^{-2} d^{-1} to 53 mmol O_2 m^{-2} d^{-1} (Walsby et al. 2001). In the small Lake Bromont (0.45 km^2), changes in light experienced by the metalimnetic cyanobacterial population caused by a seiche induced comparatively smaller variations (up to $\pm$ 25%) in photosynthetic productivity (Pannard et al. 2011).

Irradiance within the metalimnion reached 37 μmol m^{-2} s^{-1} on the sunniest days, which falls in the light range of 20–200 μmol m^{-2} s^{-1} that would support maximal growth rates of *P. rubescens* (Walsby and Schanz 2002). Most median light values in the metalimnion (3–7 μmol m^{-2} s^{-1}) were above the lower limit of 2 μmol m^{-2} s^{-1} for net growth

by *P. rubescens* (Bright and Walsby 2000), but not on 13 and 15 July. Negative photosynthetic rates were obtained on these days during which part of the *P. rubescens* biomass was located close to, and even below, the compensation depth for growth. At such low irradiances, *P. rubescens* is capable of heterotrophic growth through the assimilation of amino acids (Zotina et al. 2003; Walsby and Jüttner 2006) and glucose (Salcher et al. 2013), which may have reduced oxygen stocks. Furthermore, on both days, the majority of the *Planktothrix* population was located below the neutral buoyancy depth. It is quite conceivable that the filaments would tend to float upward by increasing the gas-vesicle volume ratio through the respiration of dense carbohydrates (Walsby et al. 2004). This may also explain the relative oxygen deficit observed on each day following these episodes of heterotrophy. On 16 July, the upward movement of the *Planktothrix* layer well above the neutral buoyancy and compensation depths resulted in a return to net daily photosynthesis.

The primary production by *P. rubescens* in Lake Zurich from July to November 1995 was found to equal zero only on 4 d, when most of the population was located below 15 m (Micheletti et al. 1998). These daily photosynthesis calculations were based on the parameter set 3 that included a higher P_m value than reported in other works (*see* Table 1), mainly because it was determined in incubation chambers containing other photosynthetic organisms (Bright and Walsby 2000). Likewise, when using the parameters of Micheletti et al. (1998), our daily photosynthesis values were nine times higher and no negative values were obtained (Table 3). Hence, it is likely that the daily photosynthesis values calculated for the 1995 growth season are overestimated compared with subsequent studies. This implies that much more negative photosynthetic rates may have occurred during that 4 month period. This is further confirmed by Walsby (2001), who recalculated the daily photosynthetic rates using a more conservative P_m value and concluded that positive production occurred most of the time, except on six occasions, during the 4 months of their weekly sampling campaign. Our high-resolution sampling indicated drastic changes in daily photosynthetic rates in Lake Zurich, from positive primary production on a given day, to negative values on the next one.

The cross-sectional lake views obtained from our robotic platform illustrated the considerable effect of seiche-induced movements on photosynthetic rates by a metalimnetic cyanobacterial species. The daily photosynthetic rates varied by two-fold for a given day, depending on the collection time of the data that were used for the calculations. The lake system was also shown to alternate between an autotrophic and heterotrophic state at daily time scales, but the frequency of heterotrophic episodes as well as their occurrence at the basin scale are still unresolved. These observations stressed the influence of the sampling time, location, and area on photosynthetic rate calculations. Clearly, the dynamic and patchy nature of cyanobacterial distribution complicates the design of an efficient sampling strategy that would give a representative monitoring. A recent review on marine harmful-bloom surveillance recommended to gather several data types (point data, transects, synoptic) from both water samples and sensors, and to collect them using various systems (i.e., ships, fixed buoys, autonomous underwater vehicles, and satellites) to improve predictive models (Stumpf et al. 2010). Similarly, lake studies should include classical sampling methods as well as real-time, high-frequency data acquisition by fixed and moving autonomous robotic platforms. A step further would be the application of adaptive sampling algorithms for environmental monitoring, but this remains a rather unexplored aspect of robotics (Dunbabin and Marques 2012). The combination of traditional techniques and new technologies would eventually allow for a finer documentation of cyanobacteria abundances in time and space, which is essential to identify promoting factors, improve prediction models, and facilitate decision-making in water management.

Acknowledgments

We are grateful to all of our colleagues at the Limnological Station in Kilchberg, particularly E. Loher for his essential contribution to sampling efforts, and M. Salcher for thoughtful comments. We extend our thanks to P. Countway and two anonymous referees for their conscientious reviews and valuable comments. We also thank the Swiss National Science Foundation for supporting this work (project CR22I2-130023).

References

Agustí, S., and E. J. Philips. 1992. Light absorption by cyanobacteria: Implications of the colonial growth form. Limnol. Oceanogr. **37:** 434–441, doi:10.4319/lo.1992.37.2.0434

Alexander, R., and J. Imberger. 2009. Spatial distribution of motile phytoplankton in a stratified reservoir: The physical controls on patch formation. J. Plankton Res. **31:** 101–118, doi:10.1093/plankt/fbn101

Biggs, W. W. 2000. Principles of radiation measurements, Li-COR®. Lincoln (NE): Li-COR Biosciences [accessed 2013 April 29]. Available from: http://www.licor.com/env/pdf/light/Rad_Meas.pdf

Blom, J., J. Robinson, and F. Jüttner. 2001. High grazer toxicity of [D-Asp^3,(*E*)-Dhb^7]microcystin-RR of *Planktothrix rubescens* as compared to different microcystins. Toxicon **39:** 1923–1932, doi:10.1016/S0041-0101(01)00178-7

Blumthaler, M. 2012. Solar radiation of the High Alps, p. 11–20. *In* C. Lütz [ed.], Plants in alpine regions. Springer Vienna.

Boegman, L. 2009. Currents in stratified water bodies 2: Internal waves, p. 539–558. *In* G. E. Likens [ed.], Encyclopedia of inland waters. Academic Press.

Bossard, P., and others. 2001. Limnological description of the Lakes Zürich, Lucerne, and Cadagno. Aquat. Sci. **63:** 225–249, doi:10.1007/PL00001353

Brient, L., and others. 2008. A phycocyanin probe as a tool for monitoring cyanobacteria in freshwater bodies. J. Environ. Monit. **10:** 248–255, doi:10.1039/b714238b

Bright, D. I., and A. E. Walsby. 2000. The daily integral of growth by *Planktothrix rubescens* calculated from growth rate in culture and irradiance in Lake Zürich. New Phytol. **146:** 301–316, doi:10.1046/j.1469-8137.2000.00640.x

Caron, D. A., and others. 2008. Macro- to fine-scale spatial and temporal distributions and dynamics of phytoplankton and their environmental driving forces in a small montane lake in southern California, USA. Limnol. Oceanogr. **53:** 2333–2349, doi:10.4319/lo.2008.53.5_part_2.2333

Carraro, E., and others. 2012. Coupling high-resolution measurements to a three-dimensional lake model to assess the spatial and temporal dynamics of the cyanobacterium *Planktothrix rubescens* in a medium-sized lake. Hydrobiologia **698:** 77–95, doi:10.1007/s10750-012-1096-y

Codd, G. A., L. F. Morrison, and J. S. Metcalf. 2005. Cyanobacterial toxins: Risk management for health protection. Toxicol. Appl. Pharm. **203:** 264–272, doi:10.1016/j.taap.2004.02.016

Cuypers, Y., B. Vinçon-Leite, A. Groleau, B. Tassin, and J. Humbert. 2010. Impact of internal waves on the spatial distribution of *Planktothrix rubescens* (cyanobacteria) in an alpine lake. ISME J. **18:** 1–10.

Davis, P. A., and A. E. Walsby. 2002. Comparison of measured growth rates with those calculated from rates of photosynthesis in *Planktothrix* spp. isolated from Blelham Tarn, English Lake District. New Phytol. **156:** 225–239, doi:10.1046/j.1469-8137.2002.00495.x

Dunbabin, M., A. Grinham, and J. Udy. 2009. An autonomous surface vehicle for water quality monitoring. Australasian Conference on Robotics and Automation 2009, Sydney, Australia. [accessed 2012 February 18]. Available from: http://www.araa.asn.au/acra/acra2009/papers/pap155s1.pdf

———, and L. Marques. 2012. Robots for environmental monitoring: Significant advancements and applications. IEEE Robot. Autom. Mag. **19:** 24–39, doi:10.1109/MRA.2011.2181683

Ernst, B., S. J. Hoeger, E. O'Brien, and D. R. Dietrich. 2009. Abundance and toxicity of *Planktothrix rubescens* in the prealpine Lake Ammersee, Germany. Harmful Algae **8:** 329–342, doi:10.1016/j.hal.2008.07.006

Ferri, G., A. Manzi, F. Fornai, B. Mazzolai, C. Laschi, F. Ciuchi, and P. Dario. 2011. Design, fabrication and first sea trials of a small-sized autonomous catamaran for heavy metals monitoring in coastal waters. IEEE Int. Conf. Robot **2011:** 2406–2411.

Garneau, M.-È., A. Schnetzer, P. D. Countway, A. C. Jones, E. L. Seubert, and D. A. Caron. 2011. Examination of the seasonal dynamics of the toxic dinoflagellate *Alexandrium catenella* at Redondo Beach, California, by quantitative PCR. Appl. Environ. Microbiol. **77:** 7669–7680, doi:10.1128/AEM.06174-11

Hantke, R., and others. 1979. Der Zürichsee und seine Nachbarseen. [Lake Zurich and its neighboring lakes]. Fribourg. Office du Livre S.A.

Hitz, G., F. Pomerleau, M.-È. Garneau, C. Pradalier, T. Posch, J. Pernthaler, and R. Siegwart. 2012. Design and application of a surface vessel for autonomous inland water monitoring. IEEE Robot. Autom. Mag. **19:** 62–72, doi:10.1109/MRA.2011.2181771

Horn, W., C. H. Mortimer, and D. J. Schwab. 1986. Wind-induced internal seiches in Lake Zurich observed and modeled. Limnol. Oceanogr. **31:** 1232–1254, doi:10.4319/lo.1986.31.6.1232

Huisman, J., and F. Hulot. 2005. Population dynamics of harmful cyanobacteria: Factors affecting species composition, p. 143–176. *In* J. Huisman, H. C. P. Matthijs, and P. M. Visser [eds.], Harmful cyanobacteria. Springer.

Invitrogen 2008. Real-time PCR: From theory to practice. Invitrogen.

Kardinaal, W. E. A., L. Tonk, I. Janse, S. Hol, P. Slot, J. Huisman, and P. M. Visser. 2007. Competition for light between toxic and nontoxic strains of the harmful cyanobacterium *Microcystis*. Appl. Environ. Microbiol. **73:** 2939–2946, doi:10.1128/AEM.02892-06

Kurmayer, R., and F. Jüttner. 1999. Strategies for the coexistence of zooplankton with the toxic cyanobacterium *Planktothrix rubescens* in Lake Zurich. J. Plankton Res. **21:** 659–683, doi:10.1093/plankt/21.4.659

Leboulanger, C., U. Dorigo, S. Jacquet, B. Le Berre, G. Paolini, and J. F. Humbert. 2002. Application of a submersible spectrofluorometer for rapid monitoring of freshwater cyanobacterial blooms: A case study. Aquat. Microb. Ecol. **30:** 83–89, doi:10.3354/ame030083

McDonald, J. H. 2009. Kruskal–Wallis test and Mann–Whitney *U* test, p. 165–172, Handbook of biological statistics. Sparky House.

McQuaid, N., A. Zamyadi, M. Prevost, D. F. Bird, and S. Dorner. 2011. Use of in vivo phycocyanin fluorescence to monitor potential microcystin-producing cyanobacterial biovolume in a drinking water source. J. Environ. Monit. **13:** 455–463, doi:10.1039/c0em00163e

Micheletti, S., F. Schanz, and A. E. Walsby. 1998. The daily integral of photosynthesis by *Planktothrix rubescens* during summer stratification and autumnal mixing in Lake Zürich. New Phytol. **138:** 233–249, doi:10.1046/j.1469-8137.1998.00196.x

Moreno-Ostos, E., L. C. Pizarro, A. Basanta, and D. G. George. 2009. Spatial heterogeneity of cyanobacteria and diatoms in a thermally stratified canyon-shaped reservoir. Int. Rev. Hydrobiol. **94:** 245–257, doi:10.1002/iroh.200811123

Münnich, M., A. Wüest, and D. M. Imboden. 1992. Observation of the second vertical mode of the internal seiche in an alpine lake. Limnol. Oceanogr. **32:** 1705–1719, doi:10.4319/lo.1992.37.8.1705

Oberhaus, L., J. F. Briand, C. Leboulanger, S. Jacquet, and J. F. Humbert. 2007. Comparative effects of the quality and quantity of light and temperature on the growth of *Planktothrix agardhii* and *P. rubescens*. J. Phycol. **43:** 1191–1199, doi:10.1111/j.1529-8817.2007.00414.x

Ostermaier, V., and R. Kurmayer. 2009. Distribution and abundance of nontoxic mutants of cyanobacteria in lakes of the Alps. Microb. Ecol. **58:** 1–11, doi:10.1007/s00248-009-9484-1

Pannard, A., B. E. Beisne, D. F. Bird, J. Braun, D. Planas, and M. Bormans. 2011. Recurrent internal waves in a small lake: Potential ecological consequences for metalimnetic phytoplankton populations. Limnol. Oceanogr. **1:** 91–109.

Pobel, D., J. Robin, and J.-F. Humbert. 2011. Influence of sampling strategies on the monitoring of cyanobacteria in shallow lakes: Lessons from a case study in France. Water Res. **45:** 1005–1014, doi:10.1016/j.watres.2010.10.011

Porter, J. H., E. Nagy, T. K. Kratz, P. Hanson, S. L. Collins, and P. Arzberger. 2009. New eyes on the world: Advanced sensors for ecology. Bioscience **59:** 385–397, doi:10.1525/bio.2009.59.5.6

Posch, T., O. Köster, M. M. Salcher, and J. Pernthaler. 2012. Harmful filamentous cyanobacteria favoured by reduced water turnover with lake warming. Nat. Clim. Change **2:** 809–813, doi:10.1038/nclimate1581

Salcher, M. M., J. Pernthaler, N. Frater, and T. Posch. 2011. Vertical and longitudinal distribution patterns of different bacterioplankton populations in a canyon-shaped, deep prealpine lake. Limnol. Oceanogr. **56:** 2027–2039, doi:10.4319/lo.2011.56.6.2027

———, T. Posch, and J. Pernthaler. 2013. In situ substrate preferences of abundant bacterioplankton populations in a prealpine freshwater lake. ISME J. **7:** 896–907, doi:10.1038/ismej.2012.162

Skulberg, O. M., and R. Skulberg. 1985. Plantic species of *Oscillatoria* (Cyanophyceae) from Norway. Characterization and classification. Arch. Hydrobiol. Beih. **71:** 157–174.

Sotton, B., O. Anneville, S. Cadel-Six, I. Domaizon, S. Krys, and J. Guillard. 2011. Spatial match between *Planktothrix rubescens* and whitefish in a mesotrophic peri-alpine lake: Evidence of toxins accumulation. Harmful Algae **10:** 749–758, doi:10.1016/j.hal.2011.06.006

Stumpf, R. P., V. Fleming-Lehtinen, and E. Graneli. 2010. Integration of data for nowcasting of harmful algal blooms. Venice-Lido: OceanObs-09 Proceedings. [accessed 2012 November 28]. Available at: https://abstracts.congrex.com/scripts/jmevent/abstracts/FCXNL-09A02b-1860409-1-ppstumpf.pdf

Tengberg, A., and others. 2003. Optodes to measure oxygen in the aquatic environment. Sea Technol. **44:** 1–6.

Thomas, E. A. 1950. Auffallige biologische Folgen von Sprungschichtneigungen im Zürichsee. Schweiz. Z. Hydrol. **12:** 1–24. [Conspicuous biological effects of thermocline depressions in Lake Zurich.]

———, and E. Märki. 1949. Der heutige Zustand des Zürichsees. Mitt. Int. Ver. Theor. Angew. Limnol. **10:** 476–488. [The current status of Lake Zurich.]

Van den Wyngaert, S., M. M. Salcher, J. Pernthaler, M. Zeder, and T. Posch. 2011. Quantitative dominance of seasonally persistent filamentous cyanobacteria (*Planktothrix rubescens*) in the microbial assemblages of a temperate lake. Limnol. Oceanogr. **56:** 97–109, doi:10.4319/lo.2011.56.1.0097

Walsby, A. E. 1997. Numerical integration of phytoplankton through depth and time in a water column. New Phytol. **136:** 189–209, doi:10.1046/j.1469-8137.1997.00736.x

———. 2001. Determining the photosynthetic productivity of a stratified phytoplankton population. Aquat. Sci. **63:** 18–43.

———, Z. Dubinsky, J. C. Kromkamp, C. Lehmann, and F. Schanz. 2001. The effects of diel changes in photosynthetic coefficients and depth of *Planktothrix rubescens* on the daily integral of photosynthesis in Lake Zürich. Aquat. Sci. **63:** 326–349, doi:10.1007/PL00001358

———, and D. P. Holland. 2006. Sinking velocities of phytoplankton measured on a stable density gradient by laser scanning. J. R. Soc. Interface **3:** 429–439, doi:10.1098/rsif.2005.0106

———, and F. Jüttner. 2006. The uptake of amino acids by the cyanobacterium *Planktothrix rubescens* is stimulated by light at low irradiances. FEMS Microbiol. Ecol. **58:** 14–22, doi:10.1111/j.1574-6941.2006.00143.x

———, G. Ng, C. Dunn, and P. A. Davis. 2004. Comparison of the depth where *Planktothrix rubescens* stratifies and the depth where the daily insolation supports its neutral buoyancy. New Phytol. **162:** 133–145, doi:10.1111/j.1469-8137.2004.01020.x

———, and F. Schanz. 2002. Light-dependent growth rate determines changes in the population of *Planktothrix rubescens* over the annual cycle in Lake Zürich, Switzerland. New Phytol. **154:** 671–687, doi:10.1046/j.1469-8137.2002.00401.x

Yu, H., H. Tsuno, T. Hidaka, and C. Jiao. 2010. Chemical and thermal stratification in lakes. Limnology **11:** 251–257, doi:10.1007/s10201-010-0310-8

Zeder, M., S. Van den Wyngaert, O. Köster, K. M. Felder, and J. Pernthaler. 2010. Automated quantification and sizing of unbranched filamentous cyanobacteria by model-based object-oriented image analysis. Appl. Environ. Microbiol. **76:** 1615–1622, doi:10.1128/AEM.02232-09

Zotina, T., O. Köster, and F. Jüttner. 2003. Photoheterotrophy and light-dependent uptake of organic and organic nitrogenous compounds by *Planktothrix rubescens* under low irradiance. Freshw. Biol. **48:** 1859–1872, doi:10.1046/j.1365-2427.2003.01134.x

Associate editor: Dariusz Stramski

Received: 03 February 2013
Accepted: 04 July 2013
Amended: 08 July 2013